

**TREE-RING MEASUREMENTS AS A PROXY OF GLACIER MASS  
BALANCE AT MOUNT BAKER, WASHINGTON, USA**

by

Amanda M. Doremus

A thesis submitted to the Faculty of the University of Delaware in partial fulfillment of the requirements for the degree of Master of Science in Geography

Spring 2017

© 2017 Amanda M. Doremus  
All Rights Reserved

**TREE-RING MEASUREMENTS AS A PROXY OF GLACIER MASS  
BALANCE AT MOUNT BAKER, WASHINGTON, USA**

by

Amanda M. Doremus

Approved: \_\_\_\_\_  
Michael A. O'Neal, Ph.D.  
Professor in charge of thesis on behalf of the Advisory Committee

Approved: \_\_\_\_\_  
Delphis F. Levia, Ph.D.  
Chair of the Department of Geography

Approved: \_\_\_\_\_  
Mohsen Badiy, Ph.D.  
Acting Dean of the College of Earth, Ocean, and Environment

Approved: \_\_\_\_\_  
Ann L. Ardis, Ph.D.  
Senior Vice Provost for Graduate and Professional Education

## **ACKNOWLEDGMENTS**

I want to thank several people for their support throughout these past two years. First, this experience would not have been possible without my advisor, Dr. Michael O'Neal, and committee member, Dr. Brian Hanson. Their continued effort to help students experience research out in the field is what initiated my interest and involvement in this research project. Furthermore, their assistance throughout this project has been invaluable and I thank them both for their support. I also want to thank my committee member Dr. Sara Rauscher for her guidance in this research project. The lab assistance of Hannah Gaston and Arthur Eng was instrumental in my work and I thank them for their many hours spent measuring tree cores. It has been a great experience working with the students and faculty of the Geography Department, and I want to also thank Dr. Tracy DeLiberty for all of her encouragement and advice as my undergraduate advisor, and also during my time in the department as a graduate student. Finally, my friends and family have been a great support system, and I especially want to thank my parents for their constant encouragement.

## TABLE OF CONTENTS

LIST OF TABLES .....	v
LIST OF FIGURES .....	vi
ABSTRACT .....	vii
Chapter	
1 INTRODUCTION .....	1
1.1 Study Area .....	3
2 METHODS .....	6
2.1 Tree-ring Chronology .....	6
2.2 Mass Balance Data .....	8
2.3 Climate Data .....	9
2.4 Mass Balance Reconstruction .....	10
3 RESULTS .....	12
3.1 Chronology Construction .....	12
3.2 Principal Components Analysis .....	12
3.3 Climate Correlations .....	13
3.4 Mass Balance Reconstruction .....	14
4 DISCUSSION .....	16
TABLES .....	23
FIGURES .....	28
REFERENCES .....	42

## LIST OF TABLES

Table 1: Summary of glacier mass balance data .....	23
Table 2: Summary of temperature, precipitation, and snow water equivalent data .....	24
Table 3: Summary and statistics of the final ring-width chronology. ....	25
Table 4: Pearson product-moment correlations.....	26
Table 5: Calibration and verification statistics for each of the mass balance reconstructions.....	27

## LIST OF FIGURES

Figure 1: Pacific Decadal Oscillation positive and negative phase sea surface temperature anomalies.....	28
Figure 2: Map of Easton Glacier .....	29
Figure 3: Raw-ring width measurements .....	30
Figure 4: Example of a detrended ring-width series .....	31
Figure 5: Map of the locations of glaciers used in regional analysis .....	32
Figure 6: Map of the locations of the climate data stations.....	33
Figure 7: Plot of the final ring-width chronology (AD 1770-2012).....	34
Figure 8: Easton Glacier mass balance reconstruction created from a simple linear regression.....	35
Figure 9: Easton Glacier mass balance reconstruction created from a linear regression with a logarithmic transformation and filtering applied .....	36
Figure 10: Regional mass balance reconstruction created from a simple linear regression.....	37
Figure 11: Regional mass balance reconstruction created from a linear regression with a logarithmic transformation and filtering applied.....	38
Figure 12: Comparison of the observed mass balance data and the reconstructions created from a simple linear regression for the Easton Bn and Regional Bn.....	39
Figure 13: Comparison of the observed mass balance data and the reconstructions for the Easton Bn and Regional Bn created from a linear regression with a logarithmic transformation and filtering applied.....	40
Figure 14: Final Regional Bn reconstruction in comparison to positive and negative PDO phases. ....	41

## **ABSTRACT**

A 243-year mass balance record was reconstructed for Easton Glacier at Mount Baker, Washington, USA, using annual ring-width measurements of mountain hemlock tree cores. Tree cores were collected on the lateral moraines of Easton Glacier and were measured and analyzed to create a site tree-ring chronology. The tree-ring chronology presented in this study responds to the same climatic forcings as glacier mass balance, mainly wintertime precipitation and summertime temperatures, providing validation for our linear regression model which uses the tree-ring chronology to reconstruct glacier annual net mass balance. Transformations were tested and applied to the data to improve the performance of the model, and a final mass-balance record for Easton Glacier and a regional index were created and analyzed for the period of AD 1770-2012. The final Easton Glacier and regional reconstructions explain 48% and 42%, respectively, of the variance in the mass balance data. Periods of above-average mass balance of Easton Glacier were identified between AD 1800-1820, AD 1845-1853, AD 1893-1927, and AD 1952-1985. Periods of predominately below-average mass balance were shown between AD 1780-1800, AD 1834-1844, AD 1884-1892, AD 1928-1951, and AD 1985-2005. Our record is consistent with known dated moraine positions and with other proxy records in the surrounding region. It also corresponds well with positive and negative phases of the Pacific Decadal Oscillation, emphasizing the influence of wintertime precipitation variability on the mass balance of glaciers in the North Cascades.

## **Chapter 1**

### **INTRODUCTION**

Over the past five decades, field studies in the North Cascades of northwestern Washington, USA, have focused on identifying past glacier-margin positions preserved as terminal and lateral moraines. These studies have created an extensive record of glacier-length changes covering the last few centuries (e.g., Fuller, 1980; Miller, 1969; Burke, 1972; Harper, 1992; Heikkinen, 1984; O'Neal, 2005; Leonard, 1974). Because North Cascades glaciers serve as sensitive indicators of climate change, integrating local, regional, and global climatic forcings, and responding to changes in mass balance, their overall retreat has been used as an indicator of recent warming trends (Oerlemans, 2005). However, inferring past climate based only on moraine records presents a limited view of the overall forcings that drive glacier length changes, where the higher-frequency advances and retreats are often overwritten by a glacier's coarse, overall response.

Of the many ways to unravel the detailed, annual responses of glaciers to climate forcings, tree-ring proxies have been one of the most valuable. In the Pacific Northwest, many tree species grow at elevations adjacent to the equilibrium line of glaciers, with annual growth rates sensitive to available energy in the form of temperature and growing season length. Thus, trees manifest enhanced growth with warmer summer temperatures but are hindered by winters with heavy precipitation, usually in the form of snow, which delay the start of the growing season (Peterson and

Peterson, 2001; Gedalof and Smith, 2001; Albright and Peterson, 2013). The predictable, energy-limited growth of trees responds to the same climatic variables as do the growth of glaciers, although in an inverse relationship: warmer summertime temperatures cause ablation of glacier mass due to melting, while cooler winters with heavy precipitation promote accumulation of glacier mass (Larocque and Smith, 2005; Watson and Luckman, 2004; Malcomb and Wiles, 2013; Marcinkowski and Peterson, 2015; Wood et al., 2011). By calibrating tree-ring data against known mass-balance records, a proxy of past glacier mass balance can be obtained, providing a sensitive mechanism to evaluate the geomorphic record of past glacier responses over time. Because trees can live for centuries, tree-ring measurements have been used to reconstruct glacier mass balance records extending back several hundred years (Larocque and Smith, 2005; Lewis and Smith, 2004; Watson and Luckman, 2004; Wood and Smith, 2013; Malcomb and Wiles, 2013). In the greater Pacific Northwest region, studies have used tree-ring measurements to describe century-scale glacier changes over a large portion of the region (Malcomb and Wiles, 2013; Larocque and Smith, 2005). While such tree-core analyses capture general climate of the region, their broad geographic extent misses the finer-scale climate details of site-specific glacier responses.

Our study seeks to expand the understanding of fine-scale, site-specific glacier mass-balance fluctuations over time by presenting a 243 year proxy record of mass balance for Easton Glacier on the southern flank of Mount Baker in the North Cascades Range of Washington, USA. Our proxy record was constructed using a tree-ring series based on 16 tree cores from high-elevation stands along the lateral

moraines of Easton Glacier, a well-studied glacier used in many regional and global climate reconstructions (e.g., Roe and O’Neal, 2009; Oerlemans, 2005). We combine our data with a multidecadal dataset of mass balance records at this specific location to gain insight into long-term mass balance trends. In order to assess the utility of our reconstruction, we apply our study to past ice-margin positions on Easton Glacier, where terminal moraine positions have been field-studied in considerable detail. We then extrapolate our findings to a regional scale, deriving a mass balance index using principal components analysis on Easton Glacier as well as seven other North Cascades glaciers with available mass balance data. Analysis of our specific site in comparison to trends in the broader North Cascades region allows us to interpret the sensitivity to climate of both Easton Glacier and regional glaciers, placing our results in terms of the known regional forcings identified in previous studies. We apply our mass balance reconstruction at the single-glacier level as well as the regional level, and interpret its climatic context with confidence, presenting a long-term study of this North Cascade glacier behavior.

## **1.1 Study Area**

The North Cascades span from northern Washington to southern British Columbia, and are east of the Strait of Juan de Fuca and the Puget Sound. They are part of the larger Cascades Range that reaches south into northern California. The region is climatically influenced by air masses that carry moisture from the Pacific Ocean across the mountainous landscape. The geography and topography of the area create a climate with relatively warm, dry summers and cool, wet winters. The North Cascades is of particular interest for climate studies because, as one of the snowiest

places in the world, the majority of the glaciers in the contiguous United States are found in the North Cascades (Hubley, 1956; Post, 1971).

Climate in the North Cascades is influenced by both natural and anthropogenic factors. Anthropogenic factors include greenhouse-gas-induced global warming, regional emissions and pollutants that affect the regional radiation balance via impacts on clouds and radiative scattering, and local to hyperlocal forcings created by land-use and land-cover changes that include urbanization and deforestation, the latter especially notable in this region known for its timber industry (O'Neal et al., 2009, 2010). Natural climate forcings in this region are mostly driven by oceanic variations, the most important of which are the Pacific Decadal Oscillation (PDO) and El Niño-Southern Oscillation (ENSO). Both oscillations occur in the Pacific Ocean, manifested primarily in the way that changes in sea-surface temperatures influence atmospheric pressure patterns. Sea-surface temperatures and atmospheric pressure patterns create the temperature and moisture characteristics of air masses that flow into the North Cascades, controlling regional climate (Mantua et al., 1997).

There are key differences in the timescales and regions impacted by the ENSO and the PDO. The ENSO is a winter-to-early-spring phenomenon that occasionally persists through a second winter, with a recurrence interval of two to seven years. It is best defined by changes in temperatures of the equatorial Pacific Ocean at latitudes from 5°N to 5°S and longitudes from 120°W to 170°W (Trenberth, 1997). PDO phases have a much longer timescale of 20 to 30 years and are best expressed by sea surface temperatures in the Pacific north of 20°N (Mantua et al., 1997; Figure 1).

During positive phases of the PDO, the Pacific Northwest experiences drier-than-average conditions, along with higher temperatures during the winter, while negative PDO phases are associated with wetter-than-average conditions and cooler winters in the Pacific Northwest (Mantua and Hare, 2002). The PDO is not fully understood because few of its multidecadal phases are represented by currently available historical data.

To gain a more comprehensive understanding of long-term trends in the Pacific Northwest, this study uses glacier mass balance data to examine past climate conditions, specifically focusing on Easton Glacier on Mount Baker. With a peak of 3,286 m, Mount Baker, a large stratovolcano, is the highest peak in the North Cascades. The peak of Mount Baker is covered by a 38.6 km<sup>2</sup> snowcap, making it an interesting area of study because of its large accumulation area at high elevations and because it experiences heavy wintertime precipitation due to its maritime location (Pelto and Brown, 2012; Harper, 1993). This study specifically focuses on one of Mount Baker's 12 glaciers, Easton Glacier. Easton Glacier has an area of 2.87 km<sup>2</sup>, flowing from bergschrunds at roughly 2900 m elevation on the south side of Mt. Baker to an ablating tongue that is currently at 1680 m elevation (Pelto and Brown, 2012). The tree cores discussed in the next section were collected from groves that are the highest elevation local groves growing on lateral moraines on each side of Easton Glacier. Railroad Grade Moraine (48.731°N, 121.842°W) is located to the west, with a tree grove between 1628-1695 m elevation, and Metcalfe Moraine (48.731°N, 121.831°W) is located to the east with a tree grove between 1560-1670 m elevation.

## Chapter 2

### METHODS

#### 2.1 Tree-ring Chronology

Mountain hemlock (*Tsuga mertensiana*) trees, found in subalpine environments in the North Cascades, were selected for this study because they are the dominant species growing at high elevations near Easton Glacier and have been previously shown to be responsive to climate for dendrochronology and dendroclimatology studies (Gedalof and Smith, 2001; Peterson and Peterson, 2001; Lewis and Smith, 2004). At the high elevations of our study area, these trees are positioned at the edge of their ecological amplitude and their annual growth is sensitive to seasonal and annual climate (Speer, 2010).

In summer field visits during 2013, 2014, and 2015, mountain hemlock tree cores were collected near Easton Glacier using an increment borer at breast height (Figure 2). Two cores were collected per tree, creating a total of 20 tree cores. Each core was dried and glued to a wooden mount, sanded with progressively finer levels of sandpaper until growth cells were clearly visible under a microscope, and then marked according to standard dendrochronology methods (Stokes and Smiley, 1996). Using a Velmex moveable stage with an optical linear encoder and a microscope with video capture software, annual ring widths were measured and recorded to the nearest 0.005 mm (Figure 3). Each core was measured by three individuals to assess and limit

measurement errors. Crossdating was performed manually and verified using COFECHA (Stokes and Smiley, 1996; Holmes, 1983).

Standardization was necessary in creating a final ring-width chronology from the tree core measurements. To remove biological trends (i.e., faster growth at younger organismal age and competition with mature trees), each data series was detrended with a cubic smoothing spline with 50% cutoff frequency at 2/3 the series length (Figure 4) using the dplR package for R (Bunn et al., 2016). This smoothing spline is commonly used in dendroclimatology studies to provide a natural fit when removing growth trends, while preserving low-frequency climate signals inherent in the data (Fritts, 2001; Speer, 2010). To create a final standardized site chronology, the original ring-width series were divided by the detrended series to create a dimensionless index, and these indices were then averaged together using Tukey's biweight robust mean. Tukey's biweight robust mean reduces the impact of outliers by giving them a weight of zero if they are outside a range of  $\pm 6$  standard deviations (Bunn et al., 2016).

Several statistics were calculated to test for a common signal among the cores. Statistics including interseries correlation, mean sensitivity, expressed population signal, and signal-to-noise ratio were assessed to ensure that all of the cores were representative of the site chronology and that they each showed sufficient response to climate variability. The interseries correlation value is a measure of the common signal between the ring-width series and is calculated by taking the average of the correlations between each individual series and the master chronology. These values

vary, but it is preferred that interseries correlation values are above 0.4 (NOAA Paleoclimatology, 2008). Mean sensitivity shows yearly variation in ring-width measurements and ranges from 0 to 1 with preferred values above 0.2. Lower mean sensitivity values indicate that the ring-widths are similar sizes and higher values imply that the ring-widths are more variable in size and highly responsive to climate (Speer, 2010). Expressed population signal (EPS) shows how the cores vary in common (relative to their independent, idiosyncratic variability). EPS values will normally increase with higher numbers of cores. Preferred values are above 0.85, but values within a comparable range ( $EPS > 0.80$ ) have been considered acceptable when a larger number of cores was not readily available (Speer, 2010; Wood et al., 2011; Wood and Smith, 2013). The signal-to-noise ratio (SNR) expresses the proportion of undesired signal in the data compared to the main signal being studied (Speer, 2010).

## **2.2 Mass Balance Data**

Existing observational glacier mass-balance data, necessary for reconstructing extended mass balance records from our tree-ring proxy data, were obtained for Easton Glacier and seven additional glaciers within 80 km of Easton Glacier from the World Glacier Monitoring Service (WGMS, 2016; Table 1; Figure 5). Besides proximity to Easton Glacier, the additional glaciers selected had to have at least 20 years of available data. Annual net mass balance (Bn) measurements specific to Easton Glacier were collected by the North Cascades Glacier Climate Project (NCGCP) for the period of AD 1990-2012. Measurements for the additional glaciers in the region were collected from the NCGCP, National Park Service (NPS) and United States Geological Survey (USGS) and are available for the collective period of

AD 1993-2012. In order to construct a regional index, a principal components analysis was performed on the annual Bn measurements for the eight glaciers over the period of AD 1993-2012. From this principal components analysis, the first principal component (PC1) was determined to represent the regional mass balance index.

### **2.3 Climate Data**

Tree growth and mass balance respond to the same climatic forcings (i.e., summertime temperatures and wintertime precipitation). To verify these relationships, historical climate data were obtained from three stations near Easton Glacier and correlated to both the tree-ring chronology and mass balance records (Figure 6). Temperature and precipitation data were accessed from the Western Regional Climate Center (WRCC) for Concrete PPL Fish Station #451679 for the period of AD 1925-2012 (Table 2). Snow water equivalent (SWE) data for the period of AD 1959-2012 were obtained from the United States Department of Agriculture Natural Resources Conservation Service (USDA NRCS) for Schreibers Meadow station 21A10 and Marten Lake station 21A09 (Table 2). Monthly temperature values were averaged to create spring, summer, and annual records. Monthly precipitation totals were summed to create a winter and annual record. In both the temperature and precipitation records, years with three or more months of missing data were excluded from the correlation analyses. Because the SWE data was missing numerous monthly values in several years throughout the entirety of the observed record period, in addition to calculating a seasonal SWE variable, data for the month of April, which had a more complete record, was evaluated separately. These enumerated annual and seasonal climate

variables were compared to the tree-ring chronology and mass balance records via the calculation of Pearson product-moment correlation coefficient ( $r$ ) values.

## 2.4 Mass Balance Reconstruction

Linear regression analysis was performed on the tree-ring chronology to reconstruct a mass balance record for Easton Glacier (Easton Bn) as well as a regional mass balance index (Regional Bn). A linear regression model was applied with the tree-ring chronology as the independent ( $x$ ) variable and the Easton observational mass balance measurements as the dependent ( $y$ ) for Easton Glacier (Equation 1), and PC1 as the dependent variable ( $y$ ) for the regional index (Equation 2).

$$(1) y = -3.356x + 3.142$$

$$(2) y = -8.633x + 9.053$$

After the linear regression analysis was performed without any modifications, another linear regression analysis was executed for Easton Glacier (Equation 3) and the regional index (Equation 4) with a logarithmic transformation and filtering applied to the data. The observational mass balance data was filtered to remove outliers outside of the normal range of the data (-2000 to 2000 mm/yr water equivalent).

$$(3) y = -3.444\log(x) - 0.102$$

$$(4) y = -9.099\log(x) + 0.831$$

Verification and summary statistics including Reduction of Error (RE), Spearman's  $\rho$ , and the Durbin Watson statistic were calculated to assess the performance of the reconstructions. The RE statistic, ranging from  $-\infty$  to  $+1$ , was used to determine how well the model fit the data, with  $+1$  meaning the model fit the data perfectly. Positive values indicate that the model has some predictive ability (Fritts,

2001). The Spearman's rank correlation coefficient ( $\rho$ ) values were calculated to evaluate the relationship between the observed and reconstructed records. Values closer to +1 or -1 show strong positive or negative association, respectively, between the records. Finally, the Durbin Watson statistic was calculated to check for autocorrelation in the residuals (0 = positive autocorrelation, 2 = no autocorrelation, 4 = negative autocorrelation).

## **Chapter 3**

### **RESULTS**

#### **3.1 Chronology Construction**

Statistical analysis of the 20 collected tree cores revealed that the strongest common variability occurred among 16 of the cores. The remaining cores were determined to have discrete growth responses that did not match the common signal among the remaining cores, so those cores were therefore excluded from the final chronology (Lewis and Smith, 2004). The statistics calculated on the final chronology included a series intercorrelation value of 0.49, mean sensitivity of 0.23, and EPS of 0.80 (Table 3), which are comparable to other studies with similar numbers of core samples collected from near-glacier settings (Wood and Smith, 2013; Wood et al., 2011). The master chronology spans 243 years (AD 1770-2012), where individual series ranged from 69 to 593 years (Figure 7). Although the individual series varied in length, a cutoff date of AD 1770 was applied based on calculations of expressed population signal (EPS). Before the year AD 1770, the sample depth was much lower so the chronology was not sufficiently reliable to analyze.

#### **3.2 Principal Components Analysis**

The principal components analysis on the eight mass balance records revealed that all of the glaciers loaded highly and positively on PC1, which explained 91.9% of the variance. Due to the high percentage of variance explained and similar loadings of

each of the glaciers on this principal component, we determined that the mass balances were exhibiting a coherent, regional response to regional weather. The second and third components (PC2 and PC3) only explained an additional 3.5% and 1.6% of the variance in the data.

### 3.3 Climate Correlations

The calculated Pearson product-moment correlation coefficient ( $r$ ) values support the use of our tree-ring measurements as a proxy for glacier mass balance (Table 4). The results from our correlation analyses showed that the ring-width chronology was positively correlated with annual temperature ( $r=0.48$ ,  $p<0.01$ ) and negatively correlated with annual precipitation ( $r=-0.42$ ,  $p<0.01$ ) and April SWE ( $r=-0.52$ ,  $p<0.01$  with Schriebers Meadow,  $r=-0.47$ ,  $p<0.01$  with Marten Lake). These results verify that warmer temperatures spur tree growth and heavier wintertime precipitation hinders tree growth. Conversely, the regional mass balance index (PC1) was negatively correlated with annual temperature ( $r=-0.73$ ,  $p<0.01$ ) and positively correlated with annual precipitation ( $r=0.67$ ,  $p<0.01$ ) and April SWE ( $r=0.53$  with Schriebers Meadow,  $r=0.68$ ,  $p<0.01$  with Marten Lake), indicating that warmer temperatures contribute negatively to mass balance and that precipitation, specifically in the form of snow, contributes positively to mass balance. These correlations, as well as the correlations calculated with seasonal variables, confirm that tree growth and mass balance respond to the same climate forcings, but with opposite effects (Table 4).

### 3.4 Mass Balance Reconstruction

The linear regression models were analyzed based on their results and residuals. The models performed well for both the Easton Bn (Figure 8; Figure 9) and Regional Bn (Figure 10; Figure 11) reconstructions. For the Easton Bn reconstruction, a simple linear regression resulted in an  $r^2$  value of 0.34, which increased to 0.48 with the logarithmic transformation and filtering applied (Table 5). Similarly, the simple linear regression for the Regional Bn exhibited an  $r^2$  value of 0.27, and was increased to 0.42 with the application of the logarithmic transformation and filtering (Table 5). After analyzing the linear regression results and residuals, the abovementioned transformations increased the model predictions ( $r^2$ ) while maintaining statistically significant results, and were therefore applied to the final reconstructions (Table 5). The logarithmic transformation provided a better fit of the data, and filtering was used to reduce the influence of two outlier years during which mass balance values were substantially out of the range of the years surrounding them. Due to the constrained timeframe of the observational data used in the model calibration, the data only captures the trends of the late 20<sup>th</sup> century and early 21<sup>st</sup> century (AD 1990-2012), during which there have been global increases in temperatures. Because the strongest restrictive effect of temperature on tree-growth is typically its influence on the start of the growing season, large increases in temperatures throughout the summer are less limiting compared to other factors (Fritts, 2001). Conversely, increases in summertime temperatures would still greatly reduce the mass balance of the glacier. This was taken into consideration in applying the filter to the data.

The reconstructions of Easton Bn and Regional Bn (AD 1770-2012) were verified through statistical analysis and visual comparison (Figure 12; Figure 13). The

final Easton and Regional Bn reconstructions explained 48% and 42% of the variance in the data, respectively (Table 5). The RE value calculated for the Easton Bn reconstruction was 0.324, and for the Regional Bn reconstruction was 0.279, showing that the models perform reasonably well. The Spearman's rank correlation coefficient ( $\rho$ ) values suggest that the Easton Bn ( $\rho = 0.631$ ,  $p < 0.01$ ) and Regional Bn ( $\rho = 0.616$ ,  $p < 0.01$ ) had fairly strong correlations between the observed and predicted data. The Durbin Watson statistic for the Easton Bn and Regional Bn do not show major autocorrelation, with values of 2.186 and 1.862, respectively.

## **Chapter 4**

### **DISCUSSION**

We have presented herein a 243 year mass-balance reconstruction for Easton Glacier, the longest temporal coverage of any proxy mass-balance record for Mount Baker, to our knowledge. This reconstruction is grounded in a tree-ring chronology obtained from stands of mountain hemlock flanking Easton Glacier. The tree-ring chronology shows temporal variations which correspond well to dated terminal moraine positions of Easton Glacier, as well as to independent mass balance reconstructions from the region (Watson and Luckman, 2004; Larocque and Smith, 2005; Wood et al., 2011; Malcomb and Wiles, 2013). The significant timespan covered by our mass-balance reconstruction enables us to assess changes in the mass of Easton Glacier in terms of the climate forcings that have affected our study locale over the last few centuries.

A compilation of terminus position data from previous Easton Glacier studies shows the recent history of Easton Glacier's terminal position as being in an extended position in the mid-1800s (Little Ice Age maximum), retreating in the early to mid-1900s, advancing from the 1960s to late 1980s, and beginning to retreat in the 1990s (Thomas, 1997; Long, 1953; Long, 1955; Harper, 1993). These periods of advance and retreat correspond well with the trends of our Easton Glacier mass balance reconstruction, although we note that the detailed record of high-frequency changes of

mass balance observed by our methods may be smoothed by studies using point-source dates.

In extending past the known record, our mass balance reconstruction allows for interpretation of Easton Glacier mass balance for the period of AD 1770-2012. To more easily identify periods of above- and below-average mass balance, we standardized our record by subtracting the mean of the entire period (-55.19 mm/yr water equivalent) from each reconstructed value. Our 10-year smoothing spline, fit to the standardized time series (Figure 9) revealed periods of predominately above-average mass-balance between AD 1800-1820, AD 1845-1853, AD 1893-1927, and AD 1952-1985, alternating with periods of predominately below-average mass balance between AD 1780-1800, AD 1834-1844, AD 1884-1892, AD 1928-1951, and AD 1985-2005.

The above- and below-average mass balance trends highlighted in our North Cascades regional mass-balance reconstruction are similar to those identified by other proxy records in the Pacific Northwest region (e.g., Watson and Luckman (2004) for Peyto Glacier, Larocque and Smith (2005) for the Mt. Waddington area, Wood and Smith (2013) for the Columbia Mountains, Malcomb and Wiles (2013) for the region of Washington to Alaska, Lewis and Smith (2004) for Colonel Foster and Septimus glaciers, and Marcinkowski and Peterson (2015) for South Cascade Glacier). Shared periods of largely positive mass balance between these records are found during AD 1810-1820, AD 1845-1855, AD 1875-1885, and AD 1960-1980, and common intervals of largely negative mass balance are observed between AD 1790-1800, AD

1930-1950, and AD 1985-1995. These results suggest that western North American glaciers have a generally synchronous behavior, with slight offsets in glacier responses caused by differences in glacier characteristics (e.g., hypsometry, elevation, surface area).

The temporal span and statistical significance of our regional mass balance reconstruction enables us to investigate the influence of the PDO on the multidecadal variability of Easton and other North Cascade glaciers in an unprecedented way. We find that multidecadal intervals of positive and negative mass balance in the North Cascades coincide closely with opposing phases of the PDO, fitting the expectation that negative PDO corresponds with positive mass balance in the North Cascades, and vice versa (Figure 14). Our regional mass balance reconstruction displays negative correlations with PDO indices, attained from the Joint Institute for the Study of the Atmosphere and Ocean (JISAO, 2017). Negative correlations were found between the Regional Bn reconstruction and averaged annual ( $r=-0.33$ ,  $p<0.01$ ) and averaged spring (MAM) PDO indices ( $r=-0.44$ ,  $p<0.01$ ) for the period of AD 1900-2012. Similar correlations have been found in other studies in this region, including a correlation of  $r = -0.44$  between a proxy mass balance record for Colonel Foster and Septimus glaciers and reconstructed PDO index (Lewis and Smith, 2004), a correlation of  $r = -0.36$  between a proxy snowpack record for Place Glacier and winter PDO (Wood et al., 2011), and a negative correlation reported between a proxy mass balance record for South Cascade Glacier and spring PDO index (Marcinkowski and Peterson, 2015). Comparison of positive and negative mass balance observed throughout the period of known PDO phases further emphasizes the relationship

between these two series (Figure 14). Periods of observed positive mass-balance coincide closely with probable negative PDO phases of AD 1890 to 1924 and AD 1947 to 1976 (JISAO, 2017). Likewise, periods of negative mass-balance correspond well with probable positive PDO phases of AD 1925 to 1946 and 1977 to the mid-1990s (JISAO, 2017).

Our observed correlation between PDO phases and mass balance demonstrates the importance of precipitation from PDO regimes on the mass balance variability of North Cascades glaciers. Previous work by Roe and O'Neal (2009) showed that changes in mass balance of Mount Baker glaciers are primarily caused by variations in precipitation, an outcome manifested in our ring-width measurements as a delay in the onset and duration of the spring/summer growing season, and subsequently manifested in the known advances observed during the negative PDO regimes between AD 1890-1924 and AD 1947-1976 (Roe and O'Neal, 2009; Montini, 2015). Glaciers at higher elevations, such as those on Mount Baker, receive a greater percentage of precipitation as snowfall rather than rainfall, yielding greater accumulation compared to nearby glaciers at lower elevations. While the global trends of glacier recession based on greenhouse-gas-induced temperature increase are well documented (Oerlemans, 1986; Oerlemans, 1994; Meier et al., 2003) the greater dependence of maritime glaciers, including those in the Cascades, on winter precipitation means that they may not be as sensitive to a global warming signal, as was shown in O'Neal et al. (2015).

In addition to the quasiperiodic PDO regime variations, two secular changes have been noted in the climate of the Cascades. Greenhouse-gas-induced global

warming has been detectable for several decades but has become unmistakable especially in the last 30 years (IPCC, 2014). Additionally, the massive deforestation associated with early 20<sup>th</sup> century logging has been identified as probably having a regional warming effect (O’Neal et al., 2009, 2010). It is reasonable to question whether the greater mass balance sensitivity to precipitation will continue if secular trends in warming continue unabated.

Although historic records of glacier terminus positions support our model, it is important to note that the timing and magnitude of terminus response to climate forcing is an integration of the mass balance record translated via the dynamics of each individual glacier. Glacier dynamics in turn depend on a multitude of factors that are highly variable between glaciers (Montini, 2015). The dynamics will produce a complicated, varying lag time between terminus advance and retreat with respect to the mass balance changes that drive them. Montini (2015) and Harper (1992) both observed the lag time of Easton Glacier to range from 13 to 17 years. It is thus likely that the more recent changes associated with greenhouse-gas-induced warming are only beginning to work their way into the responses of these glaciers, and each PDO phase change appears as a delayed pulse, not as a clear record of terminus position responding to direct forcing. Awareness of this lag time improves our interpretation of glacier changes in terms of terminus response and mass balance changes over time.

Although our dendroclimatology study focused on a single site, we maximized the utility of our dataset by extrapolating to other known chronologies and by creating a Regional Bn reconstruction to place our data in a regional context. Analysis of the

regional record verifies that our data, despite being focused at a single location, fits well in comparison with other proxies in the North Cascades. However, future studies could seek to expand the spatial span, number of cores, and/or species diversity of the chronology. Such examples of further studies could enhance our tree-ring chronology, but it is important to note that these types of studies are limited by the availability of high-elevation trees, near the edge of their ecological amplitude, on the lateral moraines of the glacier.

We also acknowledge the limitations of our model that is calibrated to observational mass balance measurements and realize that errors in these collected measurements will impact our reconstruction. Calibration data obtained from the North Cascades Glacier Climate Project and the National Park Service are limited to a relatively recent time period. The NCGCP and NPS have been operating since AD 1984 and 1993, respectively, and today conjointly monitor an area of 14,000 km<sup>2</sup> in which 14 glaciers can be found (Pelto and Riedel, 2001). However, these 14 glaciers cover a small portion of glaciers in the North Cascades and only have records extending two to three decades. Calibration data obtained for South Cascade Glacier from the USGS covers a slightly longer period, with measurements of mass balance starting in AD 1959, but this is still a minor timespan in the larger context of climate. Because our model is calibrated to a relatively short and recent time period, it may exert a bias towards recent climate conditions. The mass balance measurements used in this analysis span a primarily positive PDO phase, and therefore our reconstruction may also have a bias towards positive PDO (i.e., negative mass balance).

Natural (i.e., the PDO) and anthropogenic (i.e., greenhouse gases and land-use and land-cover change) factors have greatly influenced the climate, and therefore the mass balance, of Easton Glacier and other North Cascades glaciers, as seen in our mass balance reconstructions and in other North Cascades studies (O’Neal et al., 2010). Our study, representing nearly two and a half centuries of glacial mass-balance, supports the understanding that mass balance patterns strongly correspond to PDO, and shows that winter precipitation has a considerable influence on mass balance. Therefore, a sophisticated understanding of the role of Pacific Ocean “weather” on west coast North American precipitation will be required before we truly understand North Cascades glacier fluctuations.

## TABLES

Table 1: Summary of glacier mass balance data used in a principal components analysis to create a regional mass balance index. Easton Glacier mass balance data was evaluated independently as well as being used in the creation of the regional index.

<b>Glacier</b>	<b>WGMS ID<sup>1</sup></b>	<b>Region</b>	<b>Location (Latitude/Longitude)</b>	<b>Elevation Range</b>	<b>Period Used</b>	<b>Source</b>
Easton	1367	Mt. Baker	48.76°N, 121.83°W	1680-2900m	1990 - 2012	NCGCP <sup>2</sup>
Lower Curtis	77	Mt. Shuksan	48.83°N, 121.62°W	1650-1950m	1993 - 2012	NCGCP <sup>2</sup>
Noisy Creek	1666	Bacon Peak	48.67°N, 121.53°W	1800-2000m	1993 - 2012	NPS <sup>3</sup>
North Klawatti	1664	Primus Peak	48.57°N, 121.09°W	1740-2400m	1993 - 2012	NPS <sup>3</sup>
Rainbow	79	Mt. Baker	48.80°N, 121.77°W	1310-2200m	1993 - 2012	NCGCP <sup>2</sup>
Sholes	3295	Mt. Baker	48.81°N, 121.77°W	1610-2110m	1993 - 2012	NCGCP <sup>2</sup>
South Cascade	205	Sentinel Peak	48.35°N, 121.06°W	1640-2300m	1993 - 2012	USGS <sup>4</sup>
Yawning	75	Magic Mountain	48.45°N, 121.03°W	1880-2010m	1993 - 2012	NCGCP <sup>2</sup>

<sup>1</sup>World Glacier Monitoring Service ID #

<sup>2</sup>North Cascades Glacier Climate Project (NCGCP)

<sup>3</sup>National Park Service (NPS)

<sup>4</sup>United States Geological Survey (USGS)

Table 2: Summary of temperature, precipitation, and snow water equivalent data used in correlation analyses.

Station Name	Station ID	Location (Latitude/Longitude)	Elevation	Period Used	Source
Concrete PPL Fish Stn	USC00451679	48.54°N, 121.74°W	59.4m	1925 - 2012	WRCC <sup>1</sup>
Schreibers Meadow	21A10	48.70°N, 121.82°W	1036m	1959 - 2012	USDA NRCS <sup>2</sup>
Marten Lake	21A09	48.76°N, 121.72°W	1097m	1959 - 2012	USDA NRCS <sup>2</sup>

<sup>1</sup>Western Regional Climate Center (WRCC)

<sup>2</sup>United States Department of Agriculture - Natural Resources Conservation Service (USDA NRCS)

Table 3: Summary and statistics of the final ring-width chronology.

	Standard Chronology
Number of cores	16
Years	1770-2012
Interseries Correlation	0.49
Mean Sensitivity	0.23
Expressed Population Signal (EPS)	0.80
Signal-to-Noise Ratio (SNR)	4.02

Table 4: Pearson product-moment correlations calculated between the tree-ring chronology, observational mass balance data for Easton Glacier, the regional index, and seasonal and annual climate variables. All values are statistically significant ( $p < 0.01$ ) unless otherwise indicated.

Climate Variable		Standard Chronology	Easton Bn (1990-2012)	Regional Bn (1993-2012)
Temperature <sup>1</sup>	Spring (MAM)	0.37	-0.60	-0.63
	Summer (JJA)	0.35	-0.54	-0.62
	Annual (Oct - Sept)	0.48	-0.65	-0.73
Precipitation <sup>2</sup>	Winter (NDJFM)	-0.43	0.70	0.71
	Annual (Oct - Sept)	-0.42	0.68	0.67
Snow Water Equivalent				
(Schriebers Meadow)	April	-0.52	0.56*	0.53*
	Seasonal (Jan-June)	-0.58	0.66	0.64
(Marten Lake)	April	-0.47	0.63	0.68
	Seasonal (Jan-June)	-0.64	0.62	0.63

\*Not statistically significant ( $p < 0.01$ )

<sup>1</sup>Years with three or more months of missing data were excluded from analysis (i.e., 1965 and 2000)

<sup>2</sup>Years with three or more months of missing data were excluded from analysis (i.e., 1929 and 1965)

Table 5: Calibration and verification statistics for each of the mass balance reconstructions.

Calibration							Verification	
Model	Years	Equation	$r$	$r^2$	p-value	D-W Statistic <sup>c</sup>	RE <sup>d</sup>	Spearman $\rho^e$
Easton LRM <sup>a</sup>	1990 - 2012	$y = -3.356x + 3.142$	0.583	0.340	0.0035	2.042	0.340	0.587
Regional LRM <sup>a</sup>	1993 - 2012	$y = -8.633x + 9.053$	0.517	0.267	0.0196	1.422	0.267	0.573
Easton LRM <sup>b</sup>	1990 - 2012	$y = -3.444\log(x) - 0.102$	0.695	0.482	0.0005	2.186	0.324	0.631
Regional LRM <sup>b</sup>	1993 - 2012	$y = -9.099\log(x) + 0.831$	0.644	0.415	0.0039	1.862	0.279	0.616

<sup>a</sup>Linear regression model (LRM) without any transformations applied

<sup>b</sup>Linear regression model (LRM) with logarithmic transformation and filtering applied

<sup>c</sup>Durbin-Watson statistic

<sup>d</sup>Reduction of Error statistic

<sup>e</sup>Spearman's rank correlation coefficient ( $p < 0.01$ )

## FIGURES

### Pacific Decadal Oscillation (PDO)

Positive Phase

Negative Phase

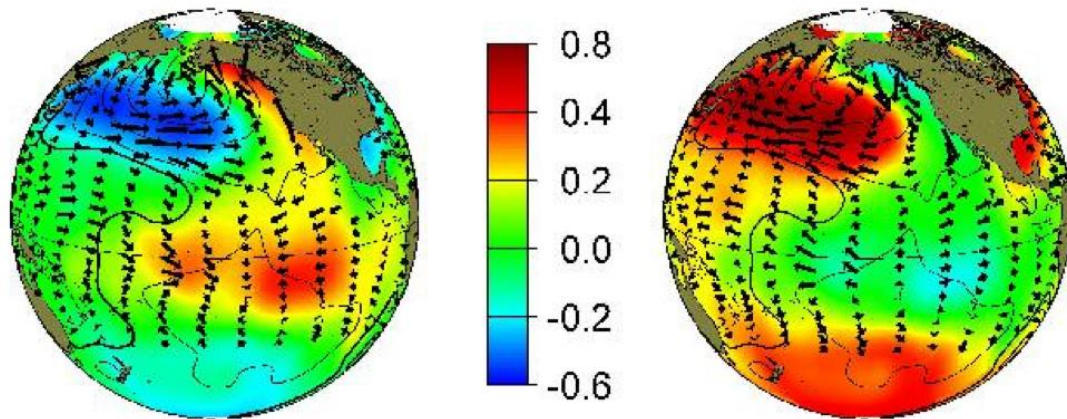


Figure 1: Pacific Decadal Oscillation positive and negative phase sea surface temperature anomalies ( $^{\circ}\text{C}$ ) (JISAO, 2017).

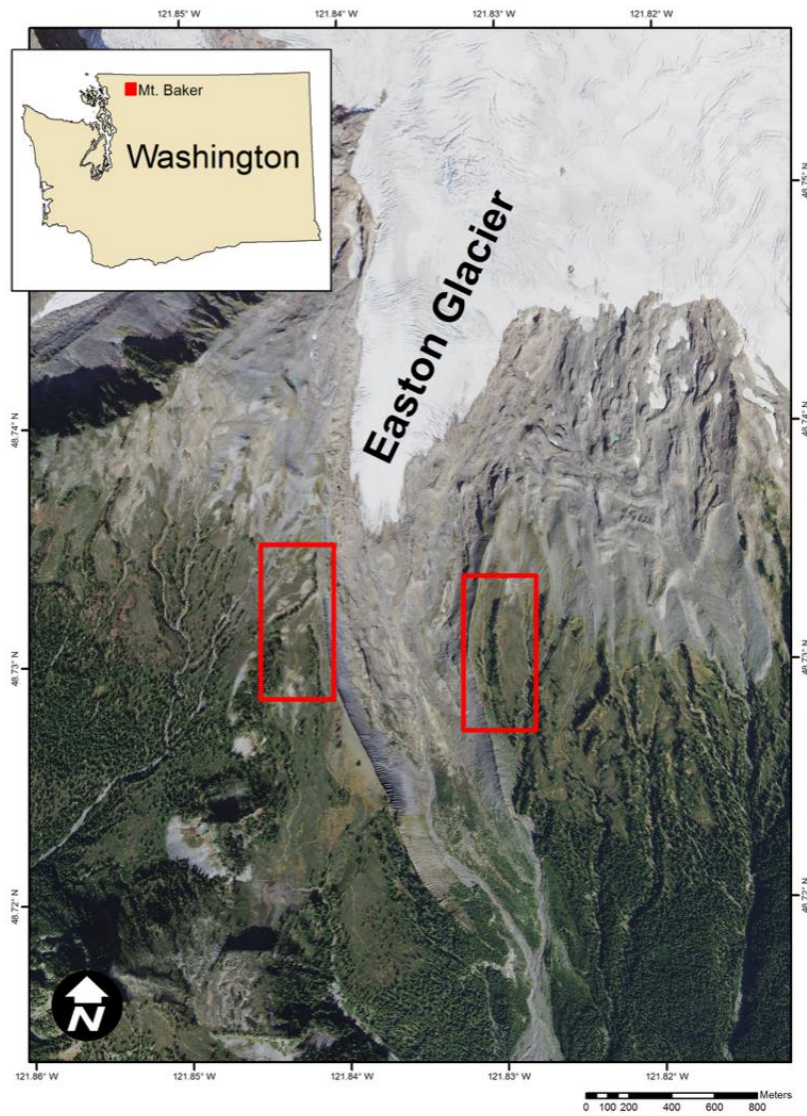


Figure 2: Map of Easton Glacier with red boxes outlining coring sites on Railroad Grade moraine to the west and Metcalfe moraine to the east. Base map is 2015 imagery from the National Agriculture Imagery Program (NAIP).

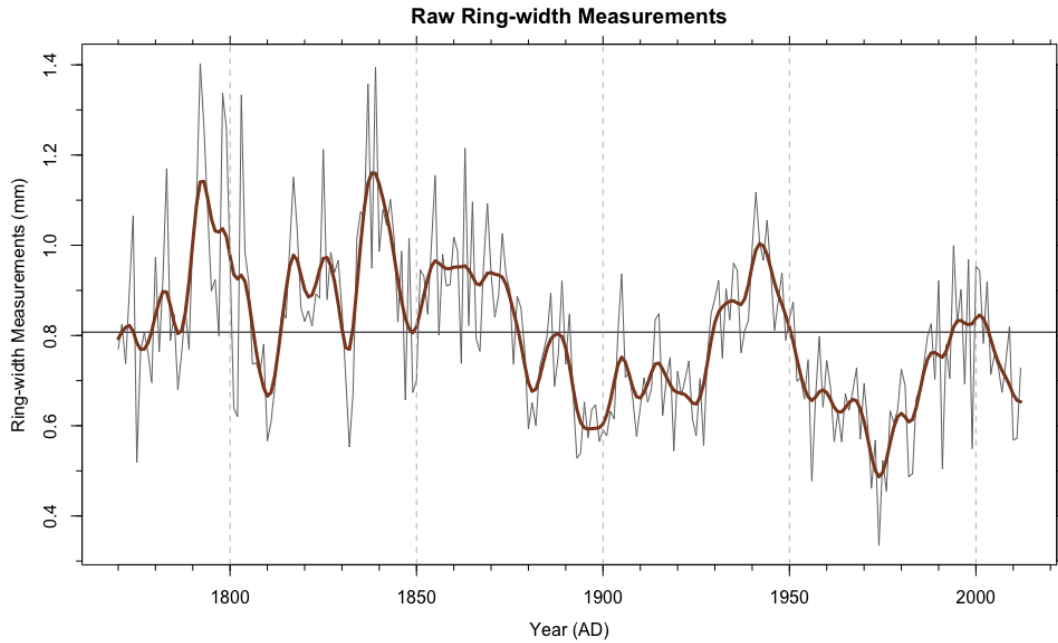


Figure 3: Raw-ring width measurements (mm) of all 16 mountain hemlock cores averaged together using Tukey's biweight robust mean. Averaged measurements are represented by the thin gray line and the thick brown line represents a 10-year smoothing spline.



Figure 4: Example of a detrended ring-width series using the dplR package in R. The top plot represents raw ring-width measurements (mm) of a single core, shown by the black line, and is fitted with a cubic smoothing spline (green curve). The bottom plot shows the standardized ring-width indices (RWI) created by detrending using the cubic smoothing spline.

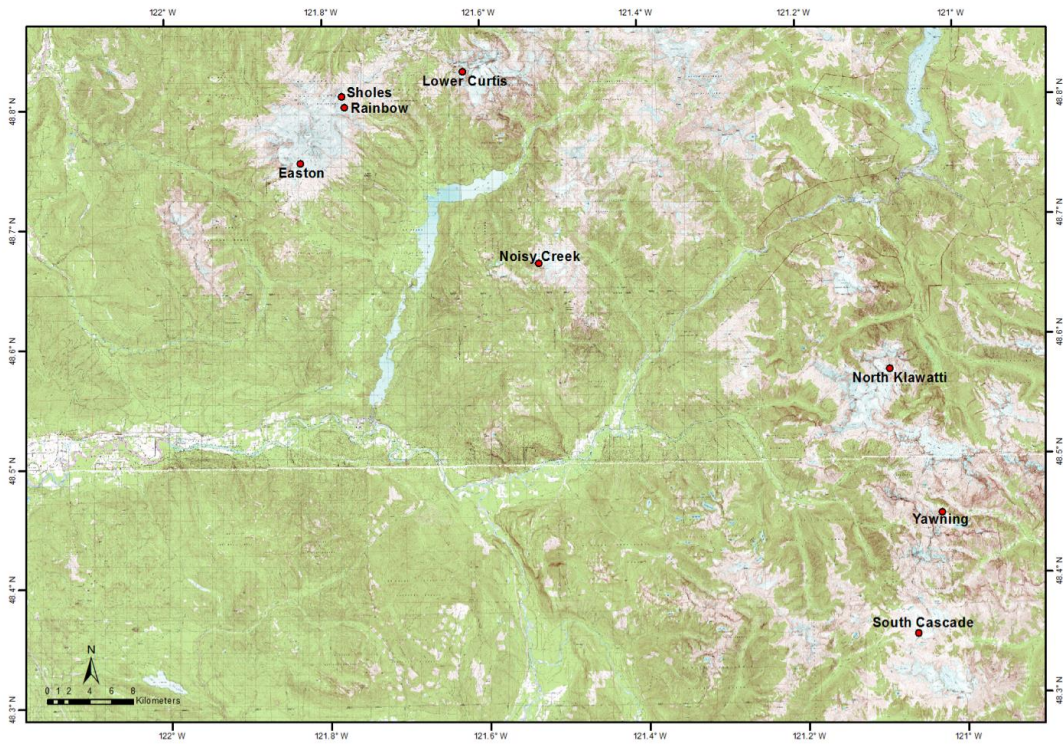


Figure 5: Map of the locations of glaciers with mass balance records that were used to create a regional mass balance index. Base map is a scanned image of a USGS topographic map and was obtained from the USDA NRCS National Cartography and Geospatial Center.

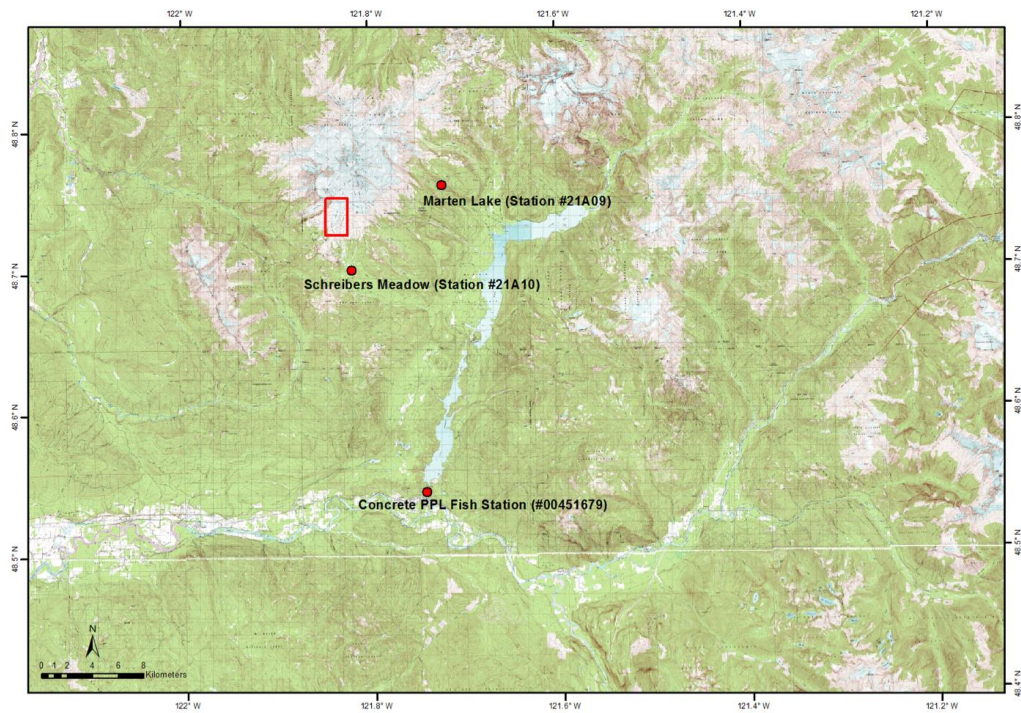


Figure 6: Map of the locations of the climate data stations. The station locations are marked by red dots and the study area is indicated by a red outline. Base map is a scanned image of a USGS topographic map and was obtained from the USDA NRCS National Cartography and Geospatial Center.

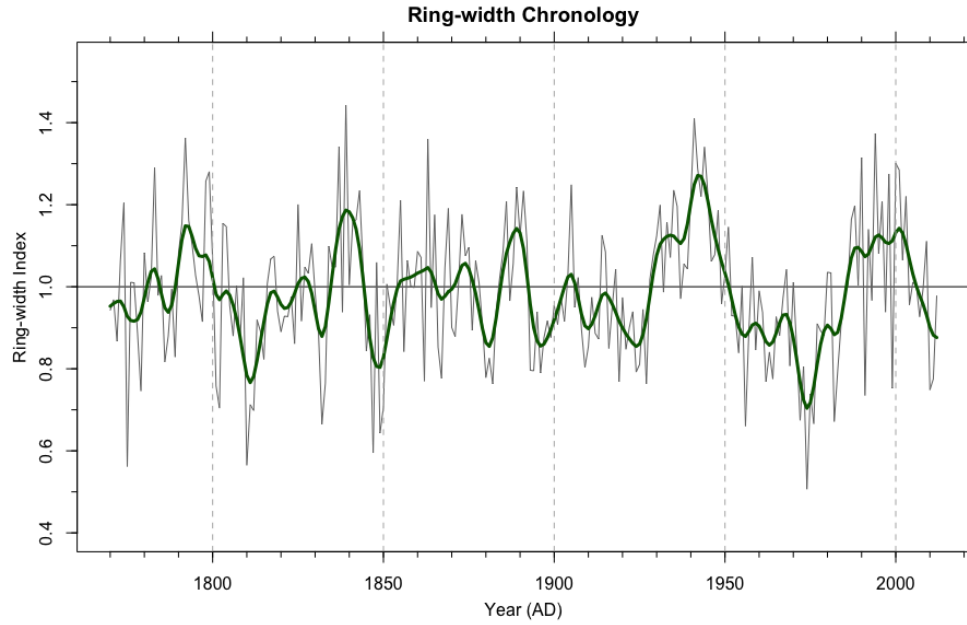


Figure 7: Plot of the final ring-width chronology indices (RWI) for the period of AD 1770-2012, created by averaging the standardized series of all the cores. The thin gray line represents the ring-width indices and the thick green line represents a 10-year smoothing spline.

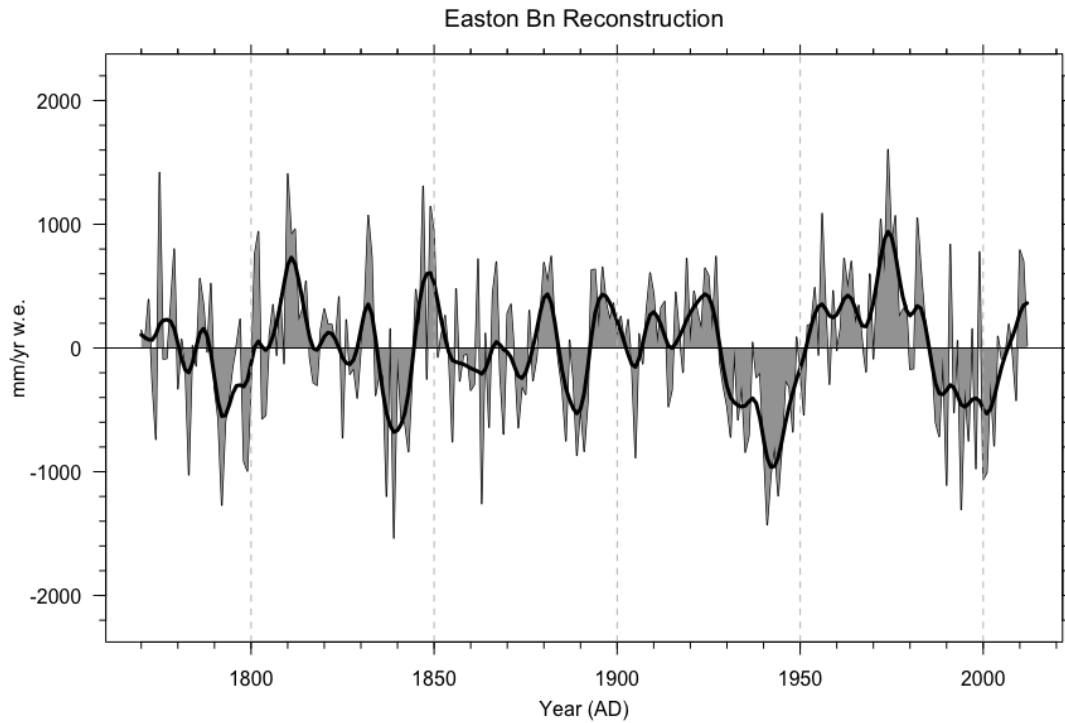
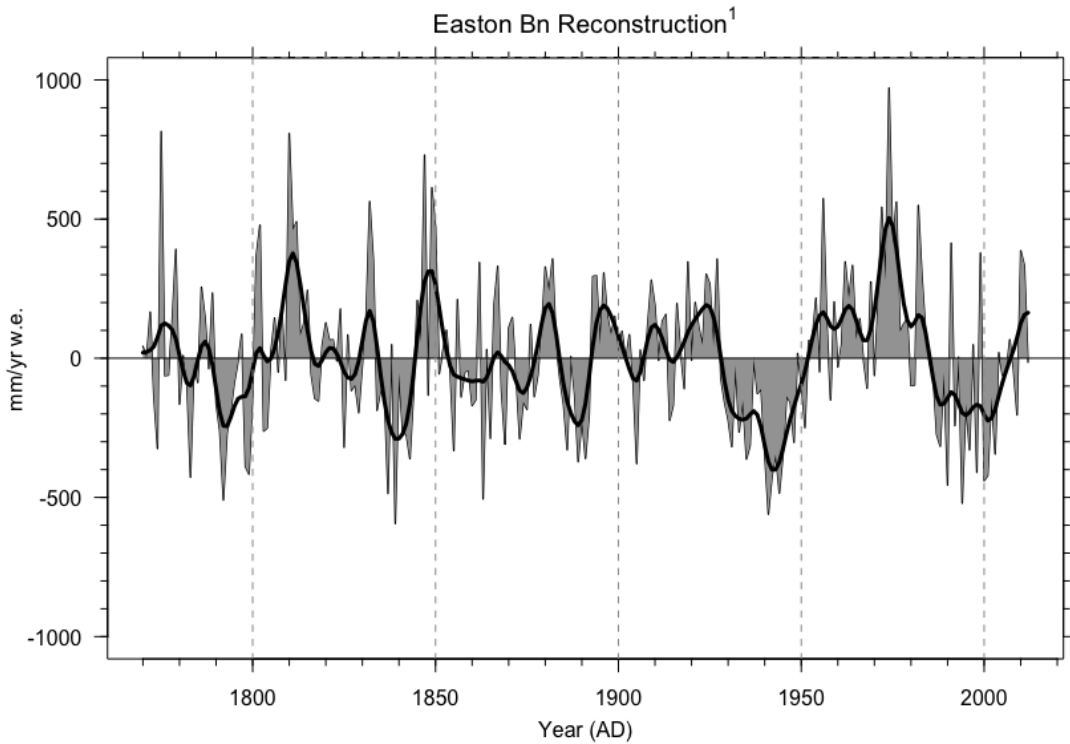


Figure 8: Easton Glacier mass balance reconstruction (mm/yr water equivalent) for the period of AD 1770-2012 created from a simple linear regression. The series was standardized by subtracting the mean of the entire period from each reconstructed value. Values above zero indicate above-average mass balance and values below zero indicate below-average mass balance. A 10-year smoothing spline is represented by the thick black line.



<sup>1</sup>Created using a linear regression model with logarithmic transformation and filtering applied.

Figure 9: Easton Glacier final mass balance reconstruction (mm/yr water equivalent) for the period of AD 1770-2012 created from a linear regression with a logarithmic transformation and filtering applied. The series was standardized by subtracting the mean of the entire period from each reconstructed value. Values above zero indicate above-average mass balance and values below zero indicate below-average mass balance. A 10-year smoothing spline is represented by the thick black line.

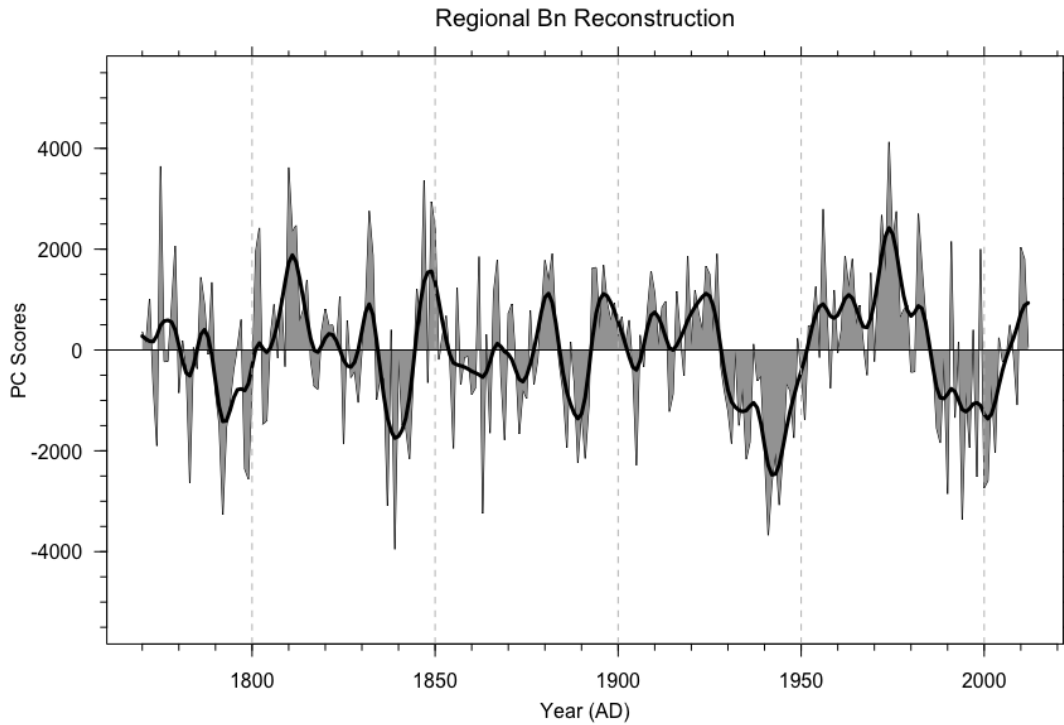
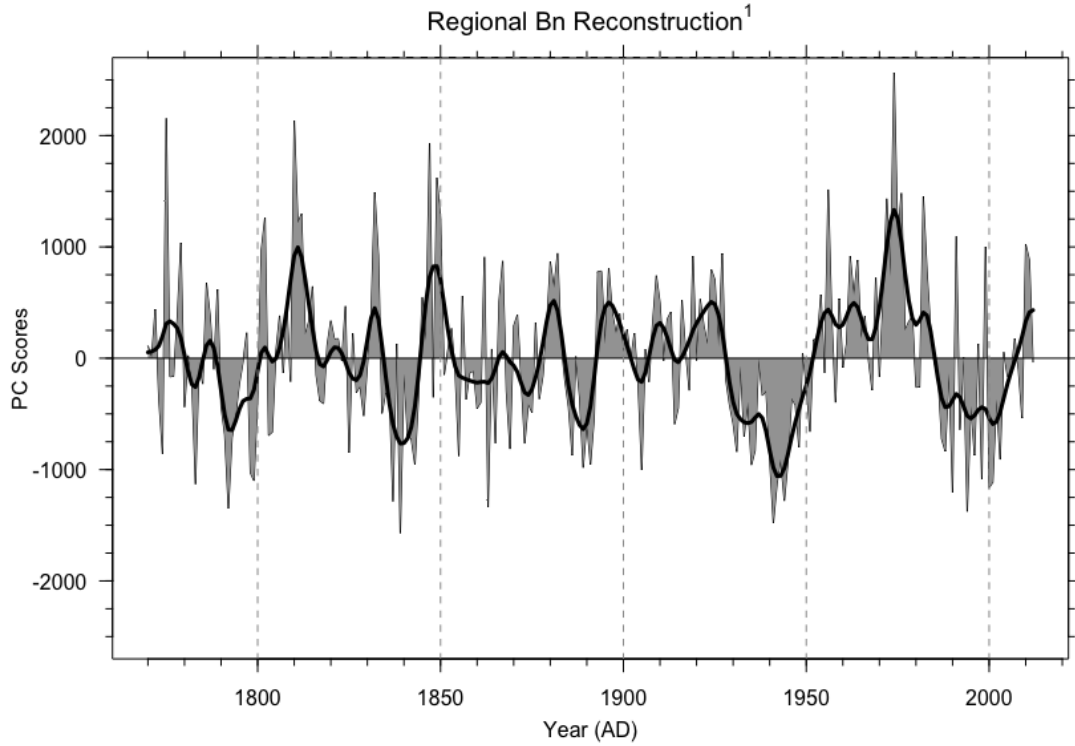


Figure 10: Regional mass balance reconstruction (PC Scores) for the period of AD 1770-2012 created from a simple linear regression. The series was standardized by subtracting the mean of the entire period from each reconstructed value. Values above zero indicate above-average mass balance and values below zero indicate below-average mass balance. A 10-year smoothing spline is represented by the thick black line.



<sup>1</sup>Created using a linear regression model with logarithmic transformation and filtering applied.

Figure 11: The final Regional mass balance reconstruction (PC Scores) for the period of AD 1770-2012 created from a linear regression with a logarithmic transformation and filtering applied. The series was standardized by subtracting the mean of the entire period from each reconstructed value. Values above zero indicate above-average mass balance and values below zero indicate below-average mass balance. A 10-year smoothing spline is represented by the thick black line.

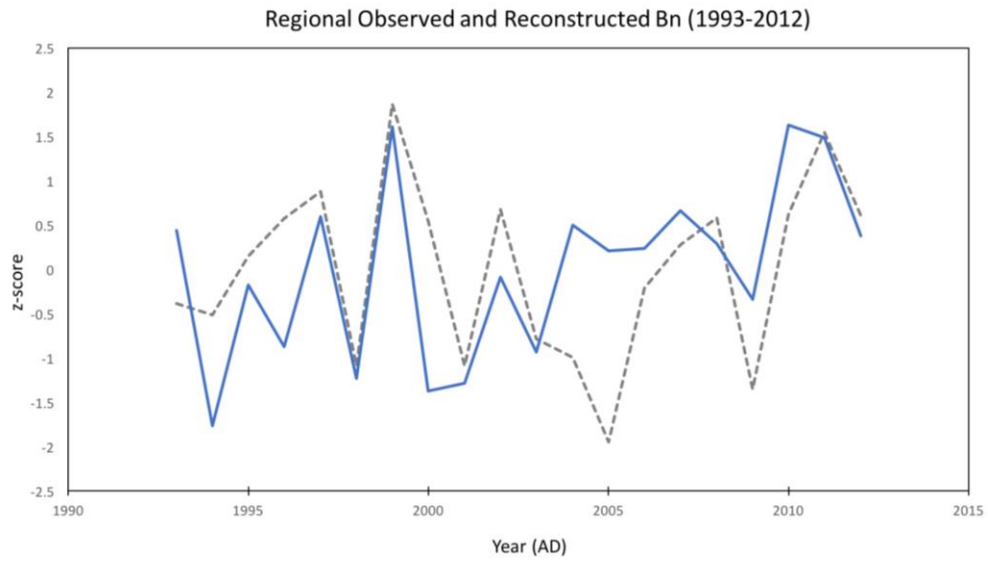
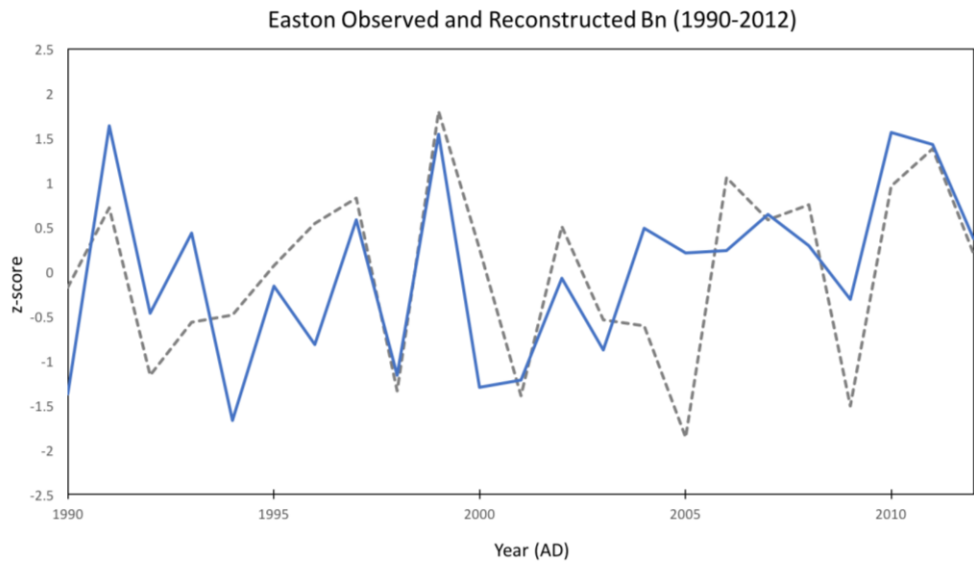
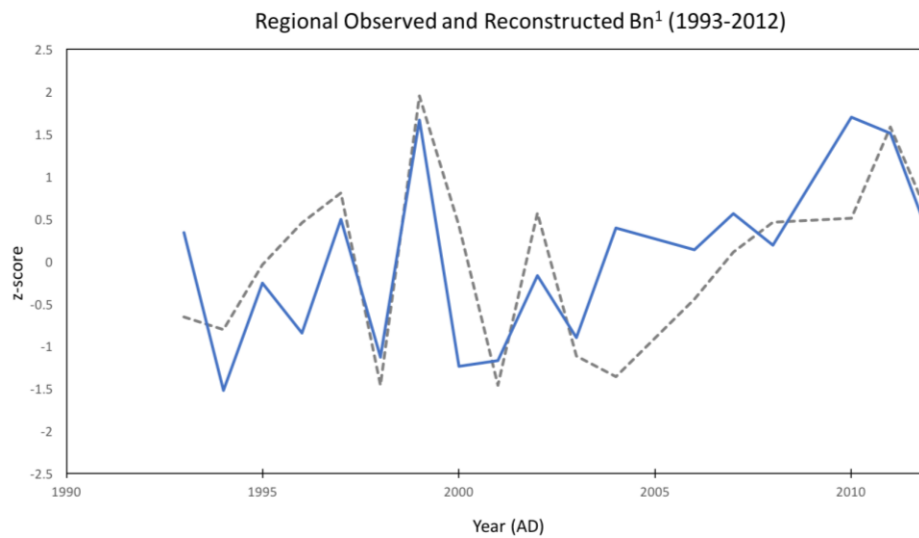
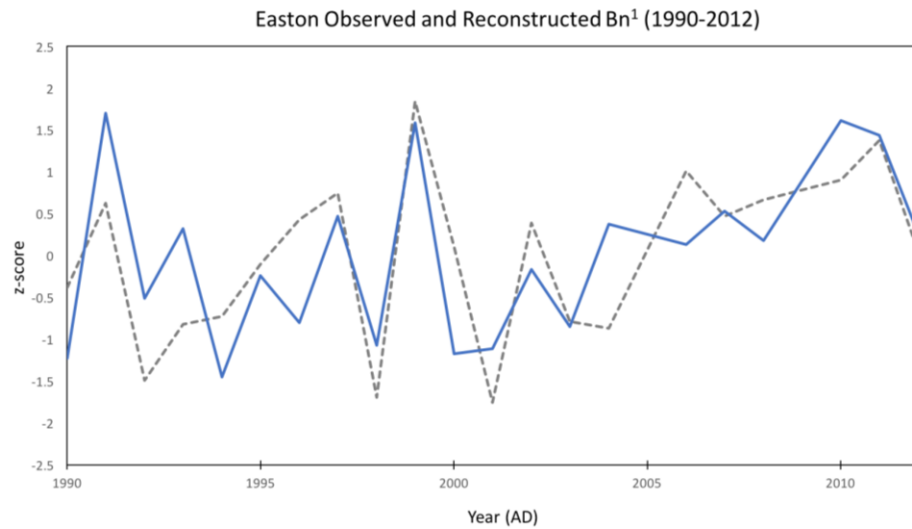


Figure 12: Comparison of the observed mass balance data and the reconstructions created from a simple linear regression for the Easton Bn and Regional Bn. Z-scores were plotted for easier comparison between the records. Z-scores of the observed data are represented by the gray dashed lines and the z-scores of the reconstructed data are represented by the solid blue lines.



<sup>1</sup>Linear regression with logarithmic transformation and filtering applied

Figure 13: Comparison of the observed mass balance data and the reconstructions for the Easton Bn and Regional Bn created from a linear regression with a logarithmic transformation and filtering applied. Z-scores were plotted for easier comparison between the records. Z-scores of the observed data are represented by the gray dashed lines and the z-scores of the reconstructed data are represented by the solid blue lines.

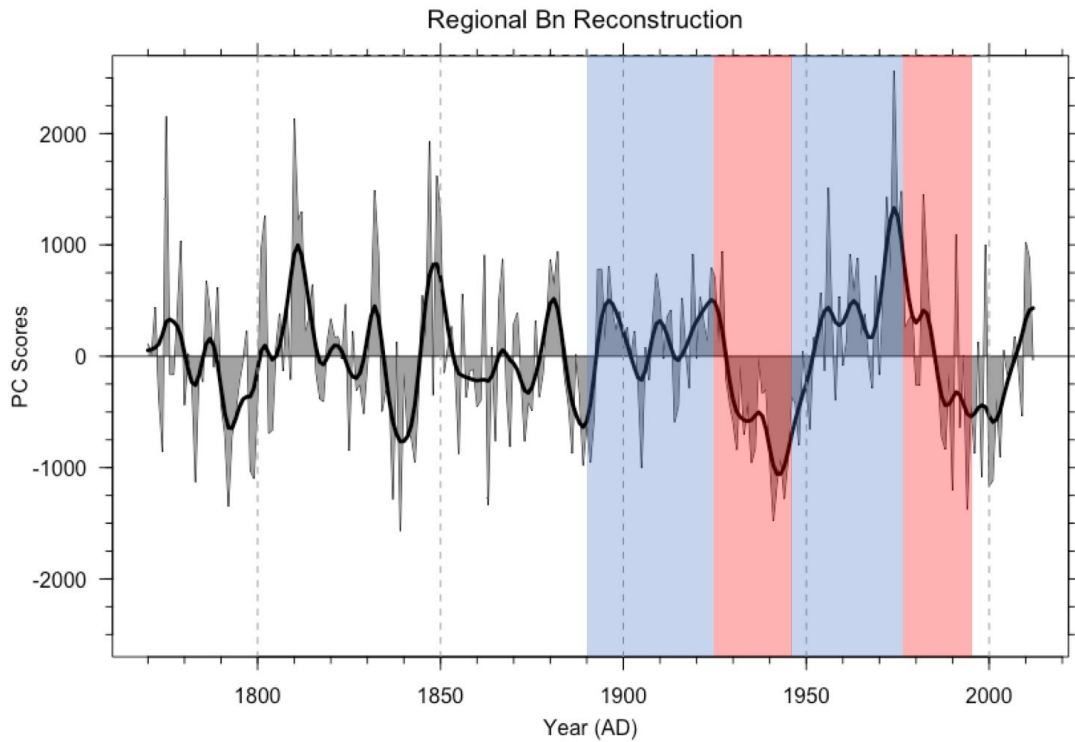


Figure 14: The final Regional Bn reconstruction (PC Scores) with transparent boxes showing positive (red) and negative (blue) PDO phases. Negative PDO regimes occur between AD 1890 to 1924 and AD 1947 to 1976 and positive PDO regimes occur between AD 1925 to 1946 and 1977 to the mid-1990s (JISAO, 2017).

## REFERENCES

- Albright WL and Peterson DL (2013) Tree growth and climate in the Pacific Northwest, North America: a broad-scale analysis of changing growth environments. Linder P (ed.), *Journal of Biogeography* 40(11): 2119–2133.
- Bunn A, Korpela M, Biondi F, et al. (2016) *dplR: Dendrochronology Program Library in R*. Available from: <https://CRAN.R-project.org/package=dplR>.
- Burke R (1972) Neoglaciatioin of Boulder Valley, Mount Baker, Washington. Bellingham: Western Washington University, p. 47.
- Fritts HC (2001) *Tree rings and climate*. Caldwell, N.J: Blackburn Press.
- Fuller SR (1980) Neoglaciatioin of Avalanche Gorge and the Middle Fork Nooksack River Valley, Mt. Baker, Washington. [Bellingham]: Western Washington University, p. 68.
- Gedalof Z and Smith DJ (2001) Dendroclimatic response of mountain hemlock (*Tsuga mertensiana*) in Pacific North America. *Canadian Journal of Forest Research* 31(2): 322–332.
- Harper JT (1992) The dynamic response of glacier termini to climatic variation during the period 1940-1990 on Mount Baker, Washington, U.S.A. Western Washington University, p. 132.
- Harper JT (1993) Glacier Terminus Fluctuations on Mount Baker, Washington, U.S.A., 1940-1990, and Climatic Variations. *Arctic and Alpine Research* 25(4): 332-340.
- Heikkinen O (1984) Dendrochronological Evidence of Variations of Coleman Glacier, Mount Baker, Washington, U.S.A. *Arctic and Alpine Research* 16(1): 53-64.
- Holmes RL (1983) Computer-Assisted Quality Control in Tree-Ring Dating and Measurement. *Tree-Ring Bulletin* 43: 69–78.
- Hubley RC (1956) Glaciers of the Washington Cascade and Olympic Mountains; their Present activity and its relation to local climatic trends. *Journal of Glaciology* 2(19): 669–674.

IPCC (2014) Climate Change 2014: Synthesis Report. Contribution of Working Groups I, II and III to the Fifth Assessment Report of the Intergovernmental Panel on Climate Change. [Core Writing Team, R.K. Pachauri and L.A. Meyer (eds.)]. IPCC, Geneva, Switzerland.

Joint Institute for the Study of the Atmosphere and Ocean (JISAO) Pacific Decadal Oscillation (PDO). Available from:  
<http://research.jisao.washington.edu/pdo/PDO.latest.txt> (accessed April 2017).

Larocque SJ and Smith DJ (2005) ‘Little Ice Age’ proxy glacier mass balance records reconstructed from tree rings in the Mt Waddington area, British Columbia Coast Mountains, Canada. *The Holocene* 15(5): 748–757.

Leonard EM (1974) Price Lake moraines: neoglacial chronology and lichenometry study. Burnaby, British Columbia: Simon Fraser University, p. 56.

Lewis D and Smith D (2004) Dendrochronological Mass Balance Reconstruction, Strathcona Provincial Park, Vancouver Island, British Columbia, Canada. *Arctic, Antarctic, and Alpine Research* 36(4): 598–606.

Long WA (1953) Recession of Easton and Deming Glaciers. *The Scientific Monthly* 76: 241–247.

Long WA (1955) What’s Happening to Our Glaciers! *The Scientific Monthly* 81(2): 57–64.

Malcomb NL and Wiles GC (2013) Tree-ring-based reconstructions of North American glacier mass balance through the Little Ice Age Contemporary warming transition. *Quaternary Research* 79(2): 123–137.

Mantua NJ and Hare SR (2002) The Pacific Decadal Oscillation. *Journal of Oceanography* 58(1) 35-44.

Mantua NJ, Hare SR, Zhang Y, et al. (1997) A Pacific Interdecadal Climate Oscillation with Impacts on Salmon Production. *Bulletin of the American Meteorological Society* 78(6): 1069–1079.

Marcinkowski K and Peterson DL (2015) A 350-Year Reconstruction of the Response of South Cascade Glacier to Interannual and Interdecadal Climatic Variability. *Northwest Science* 89(1): 14–33.

Meier MF, Dyurgerov MB and McCabe G (2003) The Health of Glaciers: Recent Changes in Glacier Regime. *Climatic Change*. 59: 123–135.

- Miller CD (1969) Chronology of neoglacial moraines in the Dome Peak area, North Cascade Range, Washington. *Arctic and Alpine Research* 1: 49–65.
- Montini TL (2015) Tree-ring-based mass balance reconstruction at Easton Glacier, Washington, USA. University of Delaware, p. 30.
- NOAA Paleoclimatology (2008) User Guide to COFECHA Output. Available from: <http://www.ncdc.noaa.gov/paleo/treering/cofecha/userguide.html> (accessed 22 June 2016).
- Oerlemans J (1986) Glaciers as indicators of the carbon dioxide warming. *Nature* 320: 607–609.
- Oerlemans J (1994) Quantifying Global Warming from the Retreat of Glaciers. *Science* 264(5156): 243–245.
- Oerlemans J (2005) Extracting a climate signal from 169 glacier records. *Science* 308: 675–677.
- O’Neal MA (2005) Late Little Ice Age glacier fluctuations in the Cascade Range of Washington and northern Oregon. Dissertation, University of Washington, p. 116.
- O’Neal MA, Hanson B, Leathers DJ, et al. (2009) Estimating Land Cover-Induced Increases in Daytime Summer Temperatures Near Mt. Adams, Washington. *Physical Geography* 30(2): 130–143.
- O’Neal MA, Roth LB, Hanson B, et al. (2010) A Field-Based Model of the Effects of Landcover Changes on Daytime Summer Temperatures in the North Cascades. *Physical Geography* 31(2): 137–155.
- O’Neal MA, Hanson B, Carisio S, et al. (2015) Detecting recent changes in the areal extent of North Cascades glaciers, USA. *Quaternary Research* 84(2): 151–158.
- Pelto M and Brown C (2012) Mass balance loss of Mount Baker, Washington glaciers 1990–2010. *Hydrological Processes* 26(17): 2601–2607.
- Pelto MS and Riedel J (2001) Spatial and temporal variations in annual balance of North Cascade glaciers, Washington 1984–2000. *Hydrological Processes* 15(18): 3461–3472.
- Peterson DW and Peterson DL (2001) Mountain Hemlock growth responds to climatic variability at annual and decadal time scales. *Ecology* 82(12): 3330–3345.

- Post A, Richardson D, Tangborn WV, et al. (1971) *Inventory of Glaciers in the North Cascades, Washington*. Professional Paper, Technical Report. Available from: <http://pubs.er.usgs.gov/publication/pp705A>.
- Roe GH and O'Neal MA (2009) The response of glaciers to intrinsic climate variability: observations and models of late-Holocene variations in the Pacific Northwest. *Journal of Glaciology* 55(193): 839–854.
- Speer JH (2010) *Fundamentals of tree-ring research*. Tucson: University of Arizona Press.
- Stokes MA and Smiley TL (1996) *An introduction to tree-ring dating*. Tucson: University of Arizona Press.
- Thomas PA (1997) Late Quaternary glaciation and volcanism on the south flank of Mt. Baker, Washington. Western Washington University, p. 98.
- Trenberth KE (1997) The Definition of El Niño. *Bulletin of the American Meteorological Society* 78(12): 2771–2777.
- Watson E and Luckman BH (2004) Tree-ring-based mass-balance estimates for the past 300 years at Peyto Glacier, Alberta, Canada. *Quaternary Research* 62(1): 9–18.
- Wood LJ and Smith DJ (2013) Climate and glacier mass balance trends from AD 1780 to present in the Columbia Mountains, British Columbia, Canada. *The Holocene* 23(5): 739–748.
- Wood LJ, Smith DJ and Demuth MN (2011) Extending the Place Glacier mass-balance record to AD 1585, using tree rings and wood density. *Quaternary Research* 76(3): 305–313.
- World Glacier Monitoring Service (2016) Fluctuations of Glaciers Database. World Glacier Monitoring Service (WGMS). Available from: <http://dx.doi.org/10.5904/wgms-fog-2016-08> (accessed 16 February 2017).